Supporting Information

Facet-Engineered Fe- and Co-Decorated Cu_2O (111) for Highly Efficient Concurrent Electrocatalytic Ammonia Synthesis and Methanol Oxidation

Chaofan Guo [a], Yan Zhang [b], Suyi Yang [a], Sheng Yang [a], Jinzhan Su*[a], Liejin Guo[a]

[a] International Research Center for Renewable Energy & State Key Laboratory of Multiphase Flow in Power Engineering, Xi'an Jiaotong University, Xi'an 710049, China

[b] State Grid Jiangxi Electric Power Research Institute, Nanchang, China

*Corresponding authors: j.su@mail.xjtu.edu.cn

S1. Experimental section

S1.1 Chemicals

$CuCl_2 \cdot 2H_2O$, NaOH, PVP, $CoCl_2 \cdot 6H_2O$, $FeCl_3 \cdot 6H_2O$ purchased from Sinopharm Chemical Reagent Co., Ltd (SCRC), All chemicals were used without further purification.

Throughout this process, PVP served as the reducing agent. By varying the ratios of $CuCl_2 \cdot H_2O$ and PVP, cuprous oxide (Cu_2O) particles featuring different crystal planes could be synthesized. Through precise control of the PVP amount, Cu_2O particles with distinct exposed crystal planes were obtained. Based on these achievements, by doping a certain proportion of $FeCl_3 \cdot 6H_2O$ and $CoCl_2 \cdot 6H_2O$, FeCo - Cu_2O catalysts could be fabricated.

S1.2 Catalyst Characterization

Scanning electron microscopy (SEM) images and energy dispersive X-ray (EDX) elemental mapping images were obtained by the JEOL JSM 7800F instrument. Transmission electron microscopy (TEM) images and high-resolution transmission electron microscopy (HRTEM) images were obtained using a FEI Tecnai G2F30 S-Twin transmission electron microscope. X-ray diffraction (XRD) and X-ray photoelectron spectroscopy (XPS) were collected by Bruker-D8 Advance and Thermo Scientific K-Alpha, respectively. The C 1s peak at 284.80 eV was used as an energy reference for all binding energies. The PL spectra was obtained by using a FLS 980 fluorescence spectrophotometer at room temperature.

S1.3. Electrochemical NRR measurement

Catalyst was employed as the working electrode, Pt foil and a Hg/HgO electrode were used as the counter electrode and reference electrode, respectively. All electrochemical tests of the catalyst samples were conducted under the same conditions using a CHI 604E electrochemical station. For the study of linear sweep voltammetry and cyclic voltammetry curves, we utilized a scan rate of 5 mV/s, and all LSV curves were corrected by 90% iR compensation to account for the influence of solution resistance. Additionally, Electrochemical Impedance Spectroscopy was employed to explore the reaction impedance with 10 mV amplitude in the frequency range 0.05 H_z to 100 KH_z. To ensure the accuracy of the experiment, nitrogen gas was flowed through the 1 M KOH solution for 30 minutes to eliminate any interference from air. Furthermore, as shown in Figure S1, the

nitrogen was purified by passing it through 0.05 M H_2SO_4 and 0.1 M KOH solutions before NRR reaction, ensuring reliable quantification of the NH_3 product in the experiment.

The electrocatalytic nitrogen reduction reaction was carried on an H-type electrolytic cell at ambient temperature and pressure (all electrochemical reactions were carried out on a CHI604E electrochemical workstation), in which the electrolytic cell was separated by a Nafion 117 membrane, which needs to underwent pre-treatment before use consisting of sonication in 5 % H_2O_2, deionized water, 0.5 M H_2SO_4, and deionized water for 20 minutes each, followed by treatment with deionized water at 80 °C for more than 12 hours. Before electrochemical testing, the cathode chamber's electrolyte underwent a 30-minute purge with N_2.

S1.4. Product Quantification:

The UV-Vis spectrophotometer was used to detect the ion concentration of pre- and post-test electrolytes after dilution to appropriate concentration to match the range of calibration curves, as shown in Figure S2.

Determination of NH_3

Concentration of produced NH_3 was determined by the indophenol blue method. In detail, 2 ml post-tested solution was removed from the cathodic chamber, and then added into 2 ml 1.0 M NaOH solution containing $C_7H_6O_3$ and $C_6H_5Na_3O_7{\cdot}2H_2O$. Next, 1ml NaClO (0.05 M) and 0.2 ml $Na_2[Fe(NO)(CN)_5]{\cdot}2H_2O$ (1 wt%) aqueous solutions were added sequentially. The mixture was allowed to stand at room temperature for 2 hours, after which the UV-Vis absorption spectrum was measured.

Determination of hydrazine (N_2H_4)

The N_2H_4 in the electrolyte was determined by UV-Vis using the Watt and Chrisp method. The -$C_9H_{11}NO$ (5.99 g), HCI (30 mL), and C_2H_5OH (300 mL) were mixed and used as a color reagent. In detail, 5 mL of electrolyte was taken from the electrochemical reaction cell, and added into 5 mL prepared color reagent and stirred for 10 min at 25 °C.

S1.5. Density functional theory (DFT) calculations

The density functional theory (DFT) calculations were carried out with the VASP code. The Perdew–Burke–Ernzerhof (PBE) functional within generalized gradient approximation (GGA) was used to process the exchange–correlation, while the projectoraugmented-wave pseudopotential (PAW)[2] was applied with a kinetic energy cut-off of 500 eV, which was utilized to describe the

expansion of the electronic eigenfunctions. The vacuum thickness was set to be 20 Å to minimize interlayer interactions. The Brillouin-zone integration was sampled by a Γ-centered 5 × 5 × 1 Monkhorst–Pack k-point. All atomic positions were fully relaxed until energy and force reached a tolerance of 1×10^{-5} eV and 0.03 eV/Å, respectively. The dispersion corrected DFT-D method was employed to consider the long-range interactions[3].

The adsorption energy (E_{ads}) of a complex formed between two molecules, A and B, can be calculated using the following equation:

$E_{ads} = E_{complex} - (E_A + E_B)$

Where: $E_{complex}$ is the total energy of the molecular complex of A and B.

E_A and E_B are the total energies of isolated molecules A and B, respectively.

The Gibbs free energy change (ΔG) was calculated by computational hydrogen electrode (CHE) model as follows:

$$\Delta G = \Delta E + \Delta ZPE - T\Delta S \quad (1)$$

where ΔE is the reaction energy obtained by the total energy difference between the reactant and product molecules absorbed on the catalyst surface and ΔS is the change in entropy for each reaction, ΔZPE is the zero-point energy correction to the Gibbs free energy. T represents room temperature (298.15 K).

S2. Figure

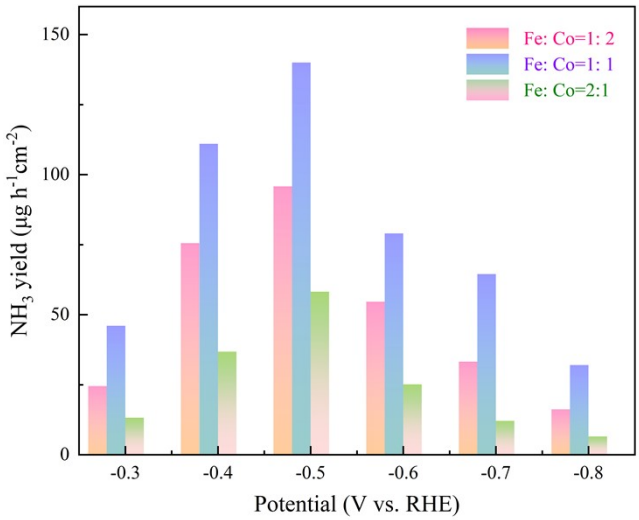

Fig. S1. Ammonia yield of catalysts with different Fe:Co ratios

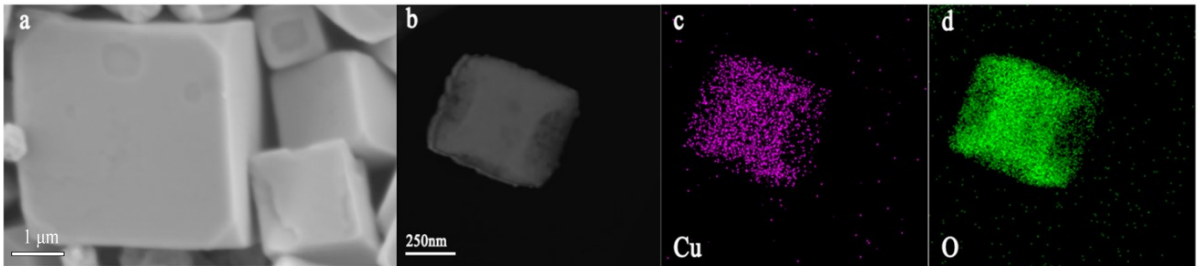

Fig. S2. (a-b) The TEM image of Cu_2O (100), (c-d) TEM-EDX image of Cu_2O (100).

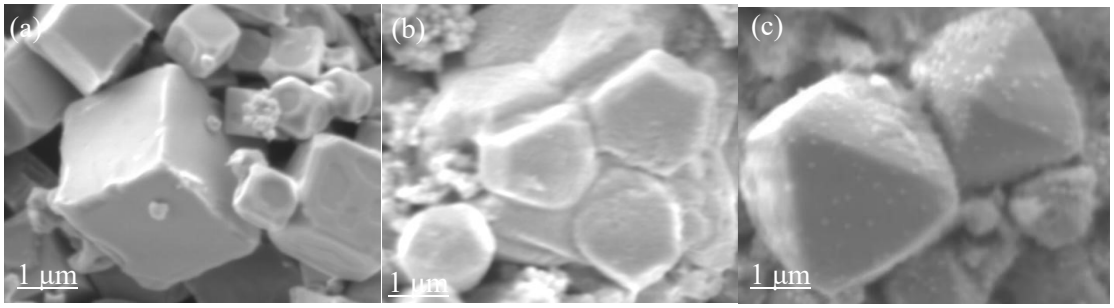

Fig. S3. The SEM image of (a) FeCo-Cu_2O (100), (b) FeCo-Cu_2O (100) & Cu_2O (111), (c) FeCo-Cu_2O (111)

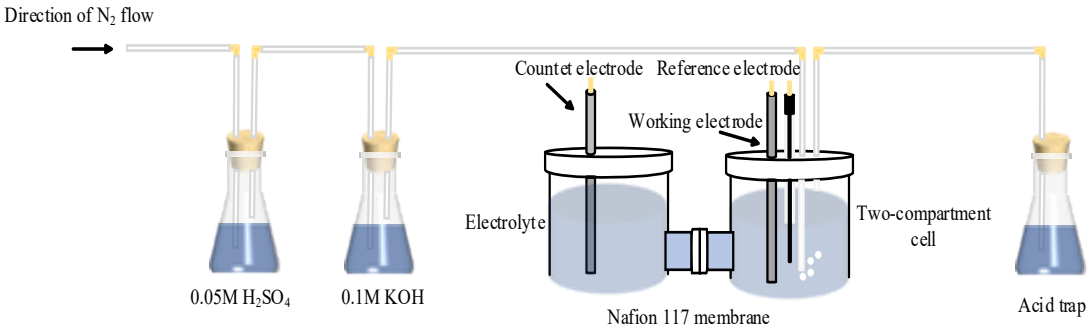

Fig. S4. Ammonia electrolysis device

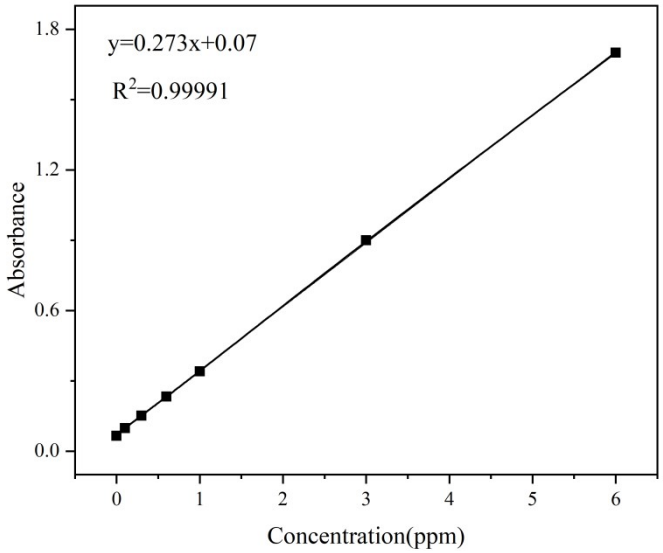

Fig. S5. Standard curve of NH_4^+

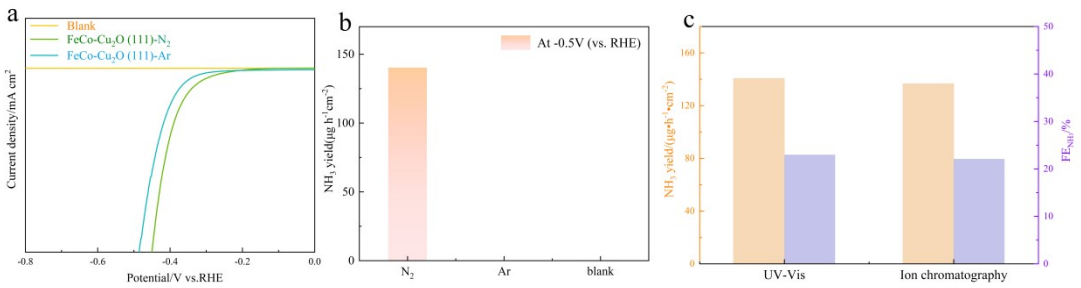

Fig. S6. (a) LSV curves in Ar- and N_2-saturated 1 M KOH solution and blank group, (b) Ammonia yield of catalysts in Ar- and N_2-saturated 1 M KOH solution and blank group, (c) UV-Vis and Ion chromatography test

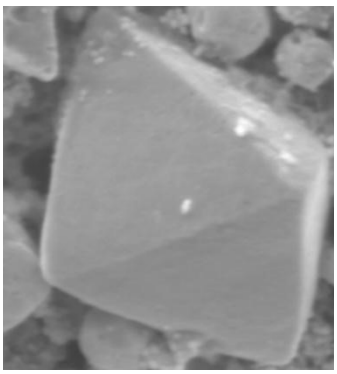

Fig. S7. SEM image of the FeCo-Cu_2O(111) after tests

S3. Table

Table S1. The comparison table of eNRR electrocatalyst performance.

electrocatalyst	Ammonia yield [μg·h^{-1}·cm^{-2}]	FE_{NH_3} [%]	Ref.
RuSAs/N-C	120.9	29.6	[5]
FeN_2B_2	115	24.8	[6]
In@Mn_3O_4	89.44	27.01	[7]
Sb-SA/N-$Ti_3C_2T_x$	108.3	41.2	[8]
$Ti_3C_2T_x$/$BiCuS_{2.5}$	62.57	67.69	[9]
MQDs/Cu	78.5	21.3	[10]
MV-MoN@NC	76.9	6.9	[11]
$CeMnO_x$	82.8	37.3	[12]
NC/BiSAs/TiN/CC	76.15	24.6	[13]
Ni_3Sn	70.60	38	[14]
Sn-CeO_{2-x}	35.3	41.1	[15]
Fe@CNF-800	37.1	10．2	[16]
Sn@Ti_2CT_X/Ti_2SnC-V	28.4	15.57	[17]
Fe-Fe_3O_4	25.4	55	[18]
$Ni_{12}P_5$/FeP_4	30.8	39.9	[19]
Nb-TiO_2(110)	21.27	9.17	[20]
Fe_3C/Fe_3O_4	25	22.5	[21]

S4. References

[1] G. Kresse, J. Furthmüller, Efficiency of ab-initio total energy calculations for metals and semiconductors using a plane-wave basis set, Comp. Mater. Sci. 6 (1) (1996) 15–50.

[2] J.P. Perdew, K. Burke, M. Ernzerhof, Generalized gradient approximation made simple, Phys. Rev. Lett. 77 (18) (1996) 3865–3868.

[3] P.E. Blochl, Projector augmented-wave method, Phys Rev B Condens Matter, 50 (1994) 17953-17979.

[4] S. Grimme, Semiempirical GGA-type density functional constructed with a long-range dispersion correction, J Comput Chem, 27 (2006) 1787-1799.

[5] Tan ZHANG, Jinping LI, Yuhan SUN, Performance regulation strategies of Ru-based nitrogen reduction electrocatalysts, CIESC Journal. 74 (2023) 2264-2280.

[6] B. Chang, Z. Cao, Y. Ren, C. Chen, L. Cavallo, F. Raziq, S. Zuo, W. Zhou, Y. Han, H. Zhang, Electronic Perturbation of Isolated Fe Coordination Structure for Enhanced Nitrogen Fixation, ACS Nano. 18 (2024) 288-298.

[7] T. Wu, Y. Du, Z.-J. Zuo, S. Li, J. Wu, J. Gao, T. Mu, Y.-C. Zhang, X.-D. Zhu, In@Mn_3O_4 with Rich Interface Low-Coordination Mn Active Sites for Boosting Electrocatalytic Nitrogen Reduction, Adv. Funct. Mater. 35 (2025) 2424142.

[8] H. Gu, J. Li, X. Niu, J. Lin, L. Chen, Z. Zhang, Z. Shi, Z. Sun, Q. Liu, P. Zhang, W. Yan, Y. Wang, L. Zhang, P. Li, X. Li, D. Wang, P. Yin, W. Chen, Symmetry-Breaking p-Block Antimony Single Atoms Trigger N-Bridged Titanium Sites for Electrocatalytic Nitrogen Reduction with High Efficiency, ACS Nano. 17 (2023) 21838-21849.

[9] R. Zhang, Y. Xue, M. Ma, Y. Han, J. Tian, Cu–Bi Bimetallic Sulfides Loaded on Two-Dimensional $Ti_3C_2T_x$ MXene for Efficient Electrocatalytic Nitrogen Reduction under Ambient Conditions, Nano Lett. 24 (2024) 10297-10304.

[10] Y. Cheng, X. Li, P. Shen, Y. Guo, K. Chu, MXene Quantum Dots/Copper Nanocomposites for Synergistically Enhanced N_2 Electroreduction, Energy Environ. Mater. 6 (2023) e12268.

[11] X. Yang, F. Ling, J. Su, X. Zi, H. Zhang, H. Zhang, J. Li, M. Zhou, Y. Wang, Insights into the role of cation vacancy for significantly enhanced electrochemical nitrogen reduction, "Appl. Catal., B". 264 (2020) 118477.

[12] C. Zhang, Q. Wang, Z. Li, H. Liu, L. Zhong, J. Liu, Z. Wang, R. Wu, P. Song, W.-J. Chen, Z. Qi, C. Yan, L. Song, Q. Yan, C. Lv, Enabling Unconventional “Alternating-Distal” N_2 Reduction Pathway for Efficient Ammonia Electrosynthesis, Angew. Chem. Int. Ed. 64 (2025) e202502957.

[13] Z. Xi, K. Shi, X. Xu, P. Jing, B. Liu, R. Gao, J. Zhang, Boosting Nitrogen Reduction Reaction via Electronic Coupling of Atomically Dispersed Bismuth with Titanium Nitride Nanorods, Adv. Sci. 9 (2022) 2104245.

[14] L. Wang, H. Liu, X. Meng, C. Sun, H.-D. Liu, L. Gong, Z. Yan, J. Wang, Phase modulation of nickel-tin alloys in regulating electrocatalytic nitrogen reduction properties, Rare Met. 43 (2024) 2851-2858.

[15] Y. Xiao, X. Tan, Y. Guo, J. Chen, W. He, H. Cui, C. Wang, Surface modification of CeO_{2-x} nanorods with Sn doping for enhanced nitrogen electroreduction, J. Energy Chem. 87 (2023) 400-407.

[16] Y. Liu, E. Huixiang Ang, X. Zhong, H. Lu, J. Yang, F. Gao, C. Yu, J. Zhu, C. Zhu, Y. Zhou, F. Yang, E. Yuan, A. Yuan, Oxygen vacancy modulation in interfacial engineering Fe_3O_4 over carbon nanofiber boosting ambient electrocatalytic N2 reduction, J. Colloid Interface Sci. 652 (2023) 418-428.

[17] X. Dai, Z.-Y. Du, Y. Sun, P. Chen, X. Duan, J. Zhang, H. Li, Y. Fu, B. Jia, L. Zhang, W. Fang, J. Qiu, T. Ma, Enhancing Green Ammonia Electrosynthesis Through Tuning Sn Vacancies in Sn-Based MXene/MAX Hybrids, Nano Micro Lett. 16 (2024) 89.
[18] H. Xie, X. Zheng, Q. Feng, X. Chen, Z. Zou, Q. Wang, J. Tang, Y. Li, Y. Ling, Single-Step Synthesis of Fe−Fe_3O_4 Catalyst for Highly Efficient and Selective Electrochemical Nitrogen Reduction, ChemSusChem. 15 (2022) e202200919.
[19] X. Jiang, M. He, M. Tang, Q. Zheng, C. Xu, D. Lin, Nanostructured bimetallic Ni–Fe phosphide nanoplates as an electrocatalyst for efficient N_2 fixation under ambient conditions, J. Mater. Sci. 55 (2020) 15252-15262.
[20] Y. Gao, Y. Yang, L. Hao, S. Hong, X. Tan, T.-S. Wu, Y.-L. Soo, A.W. Robertson, Q. Yang, Z. Sun, Single Nb atom modified anatase TiO_2(110) for efficient electrocatalytic nitrogen reduction reaction, Chem Catal. 2 (2022) 2275-2288.
[21] X. Yang, Y. Tian, S. Mukherjee, K. Li, X. Chen, J. Lv, S. Liang, L.-K. Yan, G. Wu, H.-Y. Zang, Constructing Oxygen Vacancies via Engineering Heterostructured Fe_3C/Fe_3O_4 Catalysts for Electrochemical Ammonia Synthesis, Angew. Chem. Int. Ed. 62 (2023) e202304797.